Journal Pre-proof

Novel androgen receptor antagonist identified by structure-based virtual screening, structural optimization, and biological evaluation

Qin Tang, Weitao Fu, Minkui Zhang, Ercheng Wang, Lvhu Shan, Xin Chai, Jinping Pang, Xuwen Wang, Xiaohong Xu, Lei Xu, Dan Li, Rong Sheng, Tingjun Hou

PII: S0223-5234(20)30123-9

DOI: https://doi.org/10.1016/j.ejmech.2020.112156

Reference: EJMECH 112156

To appear in: *European Journal of Medicinal Chemistry*

Received Date: 23 December 2019

Revised Date: 7 February 2020

Accepted Date: 16 February 2020

Please cite this article as: Q. Tang, W. Fu, M. Zhang, E. Wang, L. Shan, X. Chai, J. Pang, X. Wang, X. Xu, L. Xu, D. Li, R. Sheng, T. Hou, Novel androgen receptor antagonist identified by structure-based virtual screening, structural optimization, and biological evaluation, *European Journal of Medicinal Chemistry* (2020), doi: https://doi.org/10.1016/j.ejmech.2020.112156.

This is a PDF file of an article that has undergone enhancements after acceptance, such as the addition of a cover page and metadata, and formatting for readability, but it is not yet the definitive version of record. This version will undergo additional copyediting, typesetting and review before it is published in its final form, but we are providing this version to give early visibility of the article. Please note that, during the production process, errors may be discovered which could affect the content, and all legal disclaimers that apply to the journal pertain.

© 2020 Published by Elsevier Masson SAS.

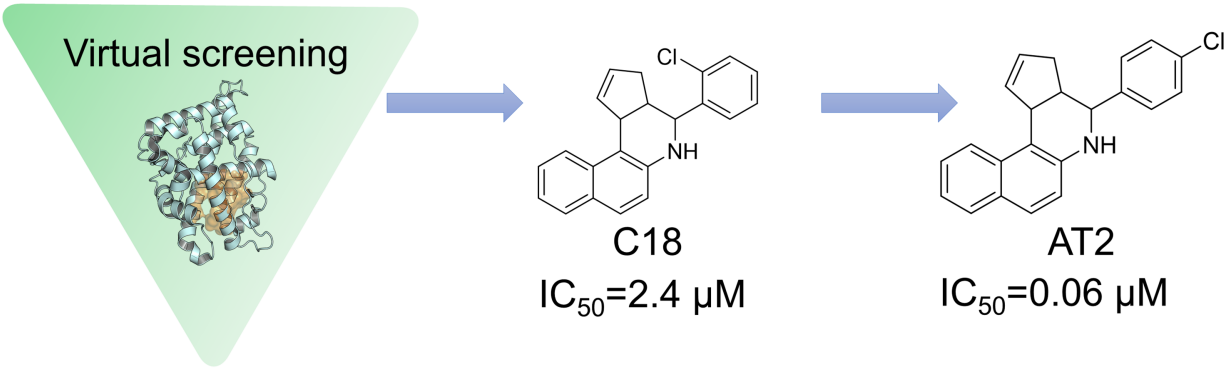

Journal Pre-proof

Journal Pre-proof

Novel androgen receptor antagonist identified by structure-based virtual screening, structural optimization, and biological evaluation

Qin Tang[1,#], Weitao Fu[1,#], Minkui Zhang[1,#], Ercheng Wang[1], Lvhu Shan[2], Xin Chai[1], Jinping Pang[1], Xuwen Wang[1], Xiaohong Xu[2], Lei Xu[3], Dan Li[1,*], Rong Sheng[1,*], Tingjun Hou[1,*]

[1]*College of Pharmaceutical Sciences, Zhejiang University, Hangzhou 310058, Zhejiang, China*

[2]*Institute of Cancer Research and Basic Medical Sciences of Chinese Academy of Sciences, Cancer Hospital of University of Chinese Academy of Sciences, Zhejiang Cancer Hospital, Hangzhou 310022, Zhejiang, China*

[3]*Institute of Bioinformatics and Medical Engineering, School of Electrical and Information Engineering, Jiangsu University of Technology, Changzhou 213001, Jiangsu, China*

[#] These authors contributed equally to this work

[*]**Corresponding authors:**

Tingjun Hou

E-mail: tingjunhou@zju.edu.cn

Rong Sheng

Email: shengrong1973@163.com

Dan Li

Email: lidancps@zju.edu.cn

Journal Pre-proof

Abstract: Androgen receptor (AR) plays important roles in the development of prostate cancer (PCa), and therefore it has been regarded as the most important therapeutic target for both hormone-sensitive prostate cancer (HSPC) and advanced PCa. In this study, a novel hit (**C18**) with IC_{50} of 2.4 μM against AR transcriptional activity in LNCaP cell was identified through structure-based virtual screening based on molecular docking and free energy calculations. The structure-activity relationship analysis and structural optimization of **C18** resulted in the discovery of a structural analogue (**AT2**), a more potent AR antagonist with 16-fold improved anti-AR potency. Further assays indicated that **AT2** was capable of effectively inhibiting the transcriptional function of AR and blocking the nuclear translocation of AR like the second generation of AR antagonists. The antagonists discovered in this study may be served as the promising lead compounds for the development of AR-driven PCa therapeutics.

Keywords: Prostate cancer; androgen receptor; structure-based virtual screening; antagonist; molecular docking

Journal Pre-proof

Journal Pre-proof

1. Introduction

Prostate cancer (PCa) is the most diagnosed cancer among men worldwide [1]. The androgen receptor (AR) is a member of the nuclear receptor superfamily of ligand-activated transcription factor. Abnormal activation of the AR signaling pathway plays a pivotal role in the development and progression of PCa [2, 3]. Currently, a vital approach to prevent the excessive activation of androgens is the treatment with AR antagonists to block the androgens binding to AR [2, 3]. Androgen deprivation therapy (ADT), the most important treatment for advanced PCa, reduces the levels of androgen production by surgical or pharmacological castration. Unfortunately, most patients usually develop into castration-resistant prostate cancer (CRPC) after 2 years of ADT treatment. The possible mechanisms of CRPC include AR mutations, AR amplifications, and active AR splice variants [4]. In general, existing studies show both PCa and CRPC are closely related to AR.

Current clinically used first-generation or second-generation AR antagonists, such as R-bicalutamide and Enzalutamide (Enz), have achieved great success against androgen-dependent PCa and improved the survival rate of PCa patients [2, 8]. However, after the initially effective response, efficacy of these AR antagonists is suffered from the rapid emergence of drug resistance [9-12]. One of the main reasons for drug resistance is the acquired point mutations at the AR LBP. An explanation for this reason is that some point mutations in the AR LBP, such as W741L, W741C, and T877 A, would create a more spacious LBP, thus converting these antagonists to agonists and inducing drug resistance [13-15]. To deal with this situation, a widely used approach in drug design is to modify the original antagonists into larger chemical structures [16-19]. Nevertheless, in general, larger molecules often confront several problems associated with unfavorable permeability and physiological distribution [20]. Therefore, it is still urgent to discover new AR antagonists with novel scaffolds to improve clinical outcomes.

A common approach to design antagonists with novel scaffolds is to use virtual screening (VS), which has also been used to identify novel hits of AR. For instance, the AR antagonist 6-(3,4-dihydro-1H-isoquinolin-2-yl)-N-(6-methylpyridin-2-yl)nicotinamide (DIMN) was screened out by structure-based VS (SBVS) based on the crystal structure of the AR-metribolone complex. Another AR antagonist 5,5a,6,10b-tetrahydroindeno[2,1-b]indole (VPC□12060) was discovered by SBVS and ligand-based virtual screening (LBVS). Wang *et al.* identified pyrazolopyramidine analogs as novel potent AR antagonists also by combining SBVS and LBVS [23]. Recently, we reported the identification of a series of novel AR ligands, including AR agonist and AR antagonist, through an integrated strategy by combining SBVS based on the crystal AR structures in complex with its agonists [24]. It has been proved that SBVS is potent to discover novel AR antagonists.

Molecular docking has been recognized as the most popular method for structure-based drug design [25-27]. It can predict the binding conformations of ligands to the target, and rank the ligands by scoring functions [28-30]. Compared with most scoring functions in molecular docking, the Molecular Mechanics/Generalized Born Surface Area (MM/GBSA) method can achieve a better balance between identifying the binding poses and predicting the binding free energies, and therefore it has been widely used in SBVS and lead optimization [31-33]. In recent years, variable dielectric MM/GBSA (VD-MM/GBSA), a novel modified MM/GBSA algorithm, has attracted increasing attention [34-37].

In this study, a multi-step SBVS strategy based on molecular docking and VD-MM/GBSA rescoring was employed to screen the Specs database, and 32 compounds were finally purchased for bioassay verification. Three of them exhibited strong bioactivities, and competitive ligand binding assay showed that 1 compound (**C18**) was targeting the LBP of AR. Structural optimization based on molecular dynamics (MD) simulation and structure-activity relationship (SAR) analysis was then applied to the hit of **C18**, which resulted in the discovery of **AT2**, a more

promising AR antagonist with 16 folds improved anti-AR potency relative to **C18**. Moreover, **AT2** displayed much better anti-proliferative effects than Enz in three androgen independent cell lines, including PC3, C4-2, and DU145. The qPCR and immunofluorescence assays illustrated that **AT2** can inhibit AR transcriptional activity and block nuclear translocation of AR. Our study provided valuable clues for the development of a novel class of AR therapeutic antagonists to combat PCa.

2. Results and discussion

*2.1. Evaluation of candidate compounds and discovery of hit **C18***

The schematic workflow of the SBVS protocol used in this study is presented in Figure 1. By applying molecular docking, VD-MM/GBSA rescoring and structural clustering, a number of potential AR antagonists were identified. As a result, a total of 32 potential active candidates were purchased and submitted to bioassays. At first, LNCaP-AR$_2$PB-eGFP-based transcriptional activity assay was performed to determine the antagonistic activities of the screened compounds at the concentration of 10 μM [24]. Compounds **C10**, **C12**, and **C18** have achieved over 50% of androgenic activity of Enz (Figure 2A and Table S1). Then, the 3 active compounds were subjected to the competitive ligand binding assay to assess their binding affinities to the LBP of the AR LBD. **C18** exhibited satisfactory binding affinity at 10 μM (Figure 2B). Thereafter, the binding affinity of **C18** at gradient concentrations was evaluated. As shown in Figure 2C, **C18** binds to the AR LBP in a dose-dependent fashion (IC_{50} = 4.02 μM), indicating that **C18** could directly target the LBP. Then the AR antagonistic activity of **C18** was evaluated. It showed that **C18** inhibited AR transcriptional activity with IC_{50} = 2.4 μM, while that for Enz was 0.08 μM (Figure 2D). To avoid potential false positive, the effect of **C18** on prostate-specific antigen (PSA), the most common used biomarker for PCa, was detected. It's observed that **C18** decreased the PSA level also in a dose-dependent manner and the IC_{50} value was 1.40 μM, while the value for Enz was 0.13 μM (Figure 2E). The structure of **C18** was then compared with the known AR antagonists deposited in the BindingDB database

Journal Pre-proof

using the *Similarity/Distance Screen* module in *Canvas* software [38]. As indicated by relatively low Tanimoto coefficient (Tanimoto coefficient < 0.3), **C18** did not share high structural similarity with any previously reported AR antagonists. Taken together, **C18** is a novel and potent AR antagonist, and can be served as a starting point for further structural optimization to improve its activity.

*2.2. Structural analysis of **C18***

To guide further structural optimization for **C18**, molecular dynamics (MD) simulations were performed to predict the dynamic binding behavior between **C18** and the AR LBD. The root-mean square deviations (RMSD) of the backbone atoms of the AR LBD and the heavy atoms of **C18** were calculated to monitor the stability of the complex during the MD simulations. As shown in Figure 3A, the RMSD evolutions for both the backbone atoms of the AR LBD and the heavy atoms of **C18** tended to converge after ~0.2 μs with the fluctuations within 1 Å (Figure 3A), suggesting the complex reached stability *via* 1 μs MD simulation. In search of the essential residues responsible for the binding of **C18** to the AR LBD, the per-residue decomposition based on VD-MM/GBSA was carried out as shown in Figure 3B. It can be found that the major contributors were Met745, Leu704, Thr877, Phe764, Leu873, Met895, Leu707, Met742, Met749, and Asn705. Most of them were hydrophobic residues around **C18** (Figure 3C). In particular, the residue Leu704 formed a hydrogen bond with the nitrogen atom of **C18**. That is to say, the antagonistic effect of **C18** was predominantly dependent on hydrophobic interactions and an important hydrogen bond with Leu704, which was highly consistent with the extremely hydrophobic feature of **C18**. According to these observations, we concluded that the alteration of different substituted groups on the phenyl ring of the R_1 moiety might lead to a rotation of the phenyl moiety or increase the probability of the formation of hydrogen bonds with Asn705 and Thr877, so as to change the antagonistic activity of the compound. The hydrophobic interactions between the AR LBD and **C18** were quite critical, and thus modification of the naphthalene ring to

Journal Pre-proof

alter hydrophobicity and introduce more hydrogen bond donors/acceptors may reinforce hydrogen bonding interaction and improve binding affinity. The 3a,4,5,11c-tetrahydro-3H-benzo[f]cyclopenta[c]quinoline ring that offers a hydrogen bond with Leu704 should be retained to maintain the anti-AR potency. Replacing the A-ring may alter the hydrophobicity, which may be favorable to improve binding affinity. Accordingly, we designed three series of **C18** analogues (**AT-CT** series, Table 1) to verify the above hypotheses.

The general strategy that may be used to improve the **AT, BT and CT** series is to alter different substituted groups R_1 moiety, alter naphthalene ring to change hydrophobicity and introduce hydrogen bond donors/acceptors, and replace A ring to alter hydrophobicity. The AT and BT series were purchased from the commercial chemical compound vendor and the CT series were synthesized by our lab (Table S2).

*2.3. Biological evaluation of the **C18** analogues*

As shown in Table 1, the effect of the substituents on the phenyl ring of the R_1 moiety was firstly examined (**AT1**-**AT8**) by AR transcriptional activity assay. It was observed that the monosubstituted compounds with smaller substituents had better activity, and the activity of the chlorine substituted compound AT2 was the best. Subsequently, the importance of the naphthalene ring was examined. The antagonistic activity was totally lost when the naphthalene ring was replaced by different R_2 groups (**BT1**-**BT7**). In addition, the contribution of the A ring was also investigated (**CT1**-**CT6**). It was found that the antagonistic activity decreased obviously when the ring A was replaced, suggesting that the cyclopentene ring is an essential component for the maintenance of bioactivity. The binding of three representative compounds (AT2, BT5, and CT5) were analyzed by molecular docking to understand why the BT series completely lost the antagonistic activity compared with the AT and CT series. As shown in Figure S1, the binding modes of AT2, BT5, and CT5 were quite similar. The docking scores for AT2, BT5 and CT5 were -11.05, -11.97, and 11.78 kcal/mol, respectively. Though the docking scores of BT5 and CT5 were comparable to that of AT2, their anti-AR

activities were significantly different. A possible explanation is that the cell membrane penetrating ability of the BT series is quite low because the AR transcriptional activities were determined at the cellular level. Another possible reason is that BT5 cannot correctly target to the AR LBD. Overall, these results suggested that alteration of the naphthalene ring with hydrogen bond donors/receptors would lead to a complete loss of the antagonistic activity, and appropriate steric hindrance and hydrophobicity are also necessary for optimal antagonistic activity.

*2.4. **AT2** is a promising AR antagonist*

The AT series (**AT1**, **AT2**, **AT4**, **AT5**, **AT6**, **AT7**, and **AT8**) were validated for their targeting ability. As shown in Figure 4A, all of the tested compounds showed relatively lower polarization values than the control of DMSO, demonstrating these compounds bound to the AR LBP effectively. Considering that **AT2** possesses optimal anti-AR transcriptional activity, the production of endogenous PSA in **AT2** treated LNCaP cells was examined. It was observed that **AT2** caused a dose-response decrease of the PSA production with IC_{50} of 0.43 μM, which was consistent with its anti-AR transcriptional activity (Figure 4B). Then, the transcriptional level of PSA was evaluated by qPCR (Figure 4C), further confirming the effect of **AT2** on PSA. In addition, another AR downstream gene transmembrane protease serine 2 (TMPRSS2) was likewise assessed. **AT2** could also dose-dependently reduce the mRNA level of TMPRSS2 (Figure 4D). Taken together, the above bioassays suggested that **AT2** could efficiently target the AR LBP and antagonize AR transcription activity. To confirm that the antagonistic effect was not induced by cytotoxicity, the viability of murine embryonic fibroblast cells (NIH□3T3 cells) exposed to **AT2** was investigated using MTT assay. Similar to Enz and **C18**, **AT2** showed no cytotoxicity against NIH□3T3 cells even at a high dose of 50 μM (Figure 4E). Thus, it could be concluded that **AT2** was nontoxic at its effective dose against AR, which confirmed the possibility of **AT2** as a candidate of AR antagonist.

Journal Pre-proof

*2.5. Inhibition of nuclear translocation of AR by **AT2***

Different from the first generation of AR antagonist, Enz is capable of blocking the translocation of AR into nucleus, which is also an important feature for the second generation of AR antagonists including the recently proved apalutamide and darolutamide [39]. To investigate the effect of **AT2** on the subcellular localization of AR, immunofluorescence was performed in LNCaP cells. As shown in Figure 5, AR was primarily cytoplasmic in the absence of DHT (DMSO), and exposure to androgen (DHT) markedly increased the nuclear-cytoplasmic ratio of AR immunofluorescence intensity, demonstrating the translocation of AR from the cytoplasm to the nucleus, while **AT2** blocked the DHT-induced AR nuclear translocation, and the corresponding results were also observed in the presence of Enz. This finding indicated that **AT2** possessed similar feature to Enz and could antagonize AR with a second-generation antagonist like mechanism.

2.6. In vitro anti-proliferative activity study

The antiproliferative potential of **AT2** was evaluated in representative androgen dependent and independent cells lines, including LNCaP, C4-2, PC3, and DU145 (Figure 6). The cell lines of LNCaP and C4-2 are known to express varying degree of AR. PC3 and Du145 are AR independent cell lines isolated from bone and brain metastatic models of human PCa, respectively. These cells were exposed to varying concentrations of Enz, **C18** and **AT2** in serum-fed condition. As shown in Figure 6A, the effect of **AT2** was comparable with that of Enz on AR-dependent cell lines of LNCaP. However, in androgen-independent C4-2 and AR-independent PC3 and DU145, **AT2** exhibited better antagonistic activity than Enz. Interestingly, the lead hit **C18** showed similar performance in C4-2 while totally different performances in AR-independent cell lines. The lead hit **C18** performed better than **AT2** in PC3, but much worse than **AT2** in DU145, suggesting that **C18** and **AT2** might exert their antiproliferative activities against PCa cell lines through a combination of AR-dependent and -independent pathways.

3. Conclusion

In this study, the SBVS strategy based on molecular docking and VD-MM/GBSA rescoring was employed to discover novel AR antagonists against PCa. A novel hit (**C18**) with promising anti-AR activities in a group of bioassays was identified. The subsequent structural optimization focusing on the change of the spatial conformations and hydrophobicity leads to a more potent AR antagonist (**AT2)** without toxicity at its effective concentration against AR. Besides, **AT2** could efficiently antagonize AR transcriptional activity, suppress downstream target gene of AR, and block the DHT-induced AR nuclear translocation as the second generation of AR antagonists. Moreover, the cytotoxicity results of **AT2** towards the cells of LNCaP, C4-2, PC3, and DU145 illustrated that **C18** and **AT2** might exert their antiproliferative activities via a combination of interfering AR-dependent and -independent pathways. Collectively, further studies on structural optimization and action mechanism of **AT2** are hopefully fruitful and will benefit the development of novel AR antagonists.

4. Methods and materials

4.1 Chemistry

*4.1.1 General synthetic procedure for compounds **CT1~CT6***

A mixture of 2-naphthylamine (**1**, 0.02 mol) and appropriate benzaldehyde (**2a-c,** 0.022 mol) in dry dichloromethane was stirred under reflux overnight. After completion of the reaction, the mixture was concentrated to give appropriate Schiff base **3a-c**, which were used directly without further purification. Then a mixture of **3a-c** (0.02 mol), 3,4-dihydro-2*H*-pyran or 2-norbornylene (0.022 mol) and indium trichloride (0.002 mol) in dichloromethane/acetonitrile (1:1, 20 mL) was stirred at room temperature overnight. After completion of the reaction, water (20 mL) was added, and the aqueous layer was extracted with dichloromethane (20 mL×3). The

combined organic layers were dried over Na_2SO_4, concentrated and purified by silica gel chromatography to give ***CT1-3*** or ***CT4-6*** (Scheme 1).

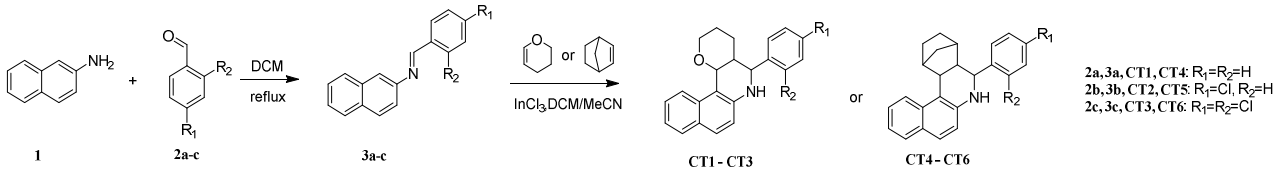

Scheme 1. Synthesis of **CT1~CT6**

*4.1.2 5-Phenyl-3,4,4a,5,6,12c-hexahydro-2H-benzo[f]pyrano[3,2-c]quinolone (**CT1**)*

White solid, yield 65%. ^{1}H NMR (500 MHz, DMSO-d_6): δ 7.76 (d, *J* = 8.5 Hz, 1H), 7.62 (d, *J* = 8.0 Hz, 1H), 7.55 (d, *J* = 9.0 Hz, 1H), 7.50 (d, *J* = 7.5 Hz, 2H), 7.42 (t, *J* = 7.5 Hz, 2H), 7.38-7.34 (m, 2H), 7.12 (t, *J* = 7.5 Hz, 1H), 6.94 (d, *J* = 9 Hz, 1H), 6.48 (s, 1H), 4.88 (d, *J* = 2.5 Hz, 1H), 4.68 (d, *J* = 11.5 Hz, 1H), 3.98 (dd, J_1 = 11 Hz, J_2 = 3.5 Hz, 1H), 3.78 (t, *J* = 11 Hz, 1H), 1.99-1.97 (m, 1H), 1.87-1.78 (m, 1H), 1.74-1.67 (m, 1H), 1.33-1.27 (m, 2H). ^{13}C NMR (125 MHz, DMSO-d_6): δ143.8, 142.8, 134.0, 129.5, 128.9, 128.6, 128.5, 128.1, 127.1, 126.8, 121.8, 121.3, 118.5, 109.9, 71.0, 68.3, 54.0, 38.5, 24.0, 21.9. HRMS (ESI): Calcd for $(M+H)^+$ ($C_{22}H_{21}NO$) 316.1701, found 316.1658.

4.1.3

*5-(4-Chlorophenyl)-3,4,4a,5,6,12c-hexahydro-2H-benzo[f]pyrano[3,2c]-quinolone (**CT2**)*

White solid, yield 62%. ^{1}H NMR (500 MHz, DMSO-d_6): δ 7.77 (d, *J* = 8.5 Hz, 1H), 7.64 (d, *J* = 7.5 Hz, 1H), 7.56 (d, *J* = 9.0 Hz, 1H), 7.53 (d, *J* = 8.5 Hz, 2H), 7.47 (t, *J* = 8 Hz, 2H), 7.39-7.36 (m, 1H), 7.13 (t, *J* = 7 Hz, 1H), 6.92 (d, *J* = 9 Hz, 1H), 6.47 (s, 1H), 4.88 (d, *J* = 2.5 Hz, 1H), 4.69 (d, *J* = 11.5 Hz, 1H), 3.98 (dd, J_1 = 9 Hz, J_2 = 3.5 Hz, 1H), 3.79 (t, *J* = 11 Hz, 1H), 1.98-1.95 (m, 1H), 1.86-1.70 (m, 2H), 1.30-1.28 (m, 2H). ^{13}C NMR (125 MHz, DMSO-d_6): δ143.6, 141.8, 134.0, 132.5, 130.4, 129.6,

Journal Pre-proof

128.9, 128.5, 127.1, 126.8, 121.9, 121.4, 118.4, 110.1, 70.8, 68.3, 53.3, 38.4, 24.0, 21.8. HRMS (ESI): Calcd for $(M+H)^+$ ($C_{22}H_{20}ClNO$) 350.1312, found 350.1316.

4.1.4

5-(2,4-Dichlorophenyl)-3,4,4a,5,6,12c-hexahydro-2*H*-benzo[*f*]pyrano[3,2-*c*]quinolone (***CT3***)

White solid, yield 68%. ^{1}H NMR (500 MHz, DMSO-d_6): δ 7.77 (d, *J* = 8.5 Hz, 1H), 7.69-7.64 (m, 3H), 7.55 (d, *J* = 8.5 Hz, 1H), 7.51 (dd, J_1 = 8.5 Hz, J_2 = 2 Hz, 1H), 7.40-7.37 (m, 1H), 7.14 (t, *J* = 7 Hz, 1H), 6.88 (d, *J* = 9 Hz, 1H), 6.51 (s, 1H), 5.17 (d, *J* = 11.5 Hz, 1H), 4.91 (d, *J* = 2.5 Hz, 1H), 3.97-3.95 (m, 1H), 3.78 (t, *J* = 9.5 Hz, 1H), 2.11-2.09 (m, 1H), 1.87-1.75 (m, 2H), 1.38-1.27 (m, 2H). ^{13}C NMR (125 MHz, DMSO-d_6): δ143.5, 139.4, 134.9, 133.9, 133.2, 131.8, 129.6, 128.9, 128.5, 127.2, 126.9, 121.9, 121.5, 118.3, 110.0, 70.8, 68.1, 49.1, 38.3, 24.0, 22.6. HRMS (ESI): Calcd for $(M+H)^+$ ($C_{22}H_{19}Cl_2NO$) 384.0922, found 384.0932.

4.1.5 5-Phenyl-1,2,3,4,4a,5,6,12c-octahydro-1,4-methanobenzo[*a*]phenanthridine (***CT4***)

White solid, yield 75%. ^{1}H NMR (500 MHz, DMSO-d_6): δ 7.69 (d, *J* = 8.5 Hz, 1H), 7.65 (d, *J* = 7.5 Hz, 1H), 7.48 (d, *J* = 8.5 Hz, 1H), 7.41-7.37 (m, 1H), 7.29 (d, *J* = 7.5 Hz, 2H), 7.23 (t, *J* = 7.5 Hz, 2H), 7.15 (t, *J* = 9 Hz, 2H), 6.96 (d, *J* = 8.5 Hz, 1H), 6.11 (s, 1H), 4.24 (d, *J* = 4 Hz, 1H), 3.14 (d, *J* = 8.5 Hz, 1H), 2.40 (s, 1H), 2.27 (dd, J_1 = 8.5 Hz, J_2 = 4 Hz, 1H), 2.24 (s, 1H), 1.73 (d, *J* = 9.5 Hz, 1H), 1.62-1.54 (m, 3H) , 1.39-1.34 (m, 1H), 0.97 (d, *J* = 9.5 Hz, 1H). ^{13}C NMR (125 MHz, DMSO-d_6): δ146.7, 143.6, 133.1, 128.9, 128.6, 128.2, 127.6, 127.3, 127.0, 126.3, 122.4, 121.4, 119.0, 115.7, 57.9, 50.1, 45.1, 43.1, 40.7, 34.7, 30.2, 29.4. HRMS (ESI): Calcd for $(M+H)^+$ ($C_{24}H_{23}N$) 326.1909, found 326.1861.

4.1.6

5-(4-Chlorophenyl)-1,2,3,4,4a,5,6,12c-octahydro-1,4-methanobenzo[a]-phenanthridi

*ne (**CT5**)*

White solid, yield 72%. ^{1}H NMR (500 MHz, DMSO-d_6): δ 7.69 (d, *J* = 8.5 Hz, 1H), 7.66 (d, *J* = 7.5 Hz, 1H), 7.48 (d, *J* = 9 Hz, 1H), 7.40-7.38 (m, 1H), 7.31-7.27 (m, 4H), 7.18-7.15 (m, 1H), 6.95 (d, *J* = 9 Hz, 1H), 6.14 (s, 1H), 4.28 (dd, J_1 = 3.5 Hz, J_2 = 2 Hz, 1H), 3.16 (d, *J* = 9 Hz, 1H), 2.38 (s, 1H), 2.26-2.24 (m, 2H), 1.71 (d, *J* = 10 Hz, 1H), 1.63-1.51 (m, 3H) , 1.40-1.36 (m, 1H), 0.96 (d, *J* = 10 Hz, 1H). ^{13}C NMR (125 MHz, DMSO-d_6): δ145.6, 143.3, 133.0, 131.5, 129.4, 128.9, 128.5, 128.3, 127.4, 126.4, 122.4, 121.5, 118.9, 115.9, 57.1, 49.9, 45.3, 43.2, 40.6, 34.7, 30.3, 29.3. HRMS (ESI): Calcd for $(M+H)^+$ ($C_{24}H_{22}ClN$) 360.1519, found 360.1523.

4.1.7

*5-(2,4-dichlorophenyl)-1,2,3,4,4a,5,6,12c-octahydro-1,4-methanobenzo[a]-phenanthridine (**CT6**)*

White solid, yield 70%. ^{1}H NMR (500 MHz, DMSO-d_6): δ 7.69 (d, *J* = 2.5 Hz, 1H), 7.67 (d, *J* = 3 Hz, 1H), 7.58 (d, *J* = 2 Hz, 1H), 7.54 (d, *J* = 9 Hz, 1H), 7.40 (t, *J* = 7.5 Hz, 1H), 7.22-7.16 (m, 2H), 7.12 (d, *J* = 8.5 Hz, 1H), 7.00 (d, *J* = 8.5 Hz, 1H), 6.22 (s, 1H), 4.63 (s, 1H), 3.14 (d, *J* = 8.5 Hz, 1H), 2.35 (s, 1H), 2.29 (s, 1H), 2.21 (d, *J* = 8.5 Hz, 1H), 1.67 (d, *J* = 9.5 Hz, 1H), 1.60-1.54 (m, 3H) , 1.42-1.37 (m, 1H), 0.98 (d, *J* = 9.5 Hz, 1H). ^{13}C NMR (125 MHz, DMSO-d_6): δ143.1, 143.0, 133.6, 132.9, 132.1, 129.3, 129.2, 129.0, 128.3, 127.8, 127.7, 126.5, 122.3, 121.7, 118.5, 115.3, 54.1, 49.4, 45.9, 44.2, 40.6, 34.7, 30.5, 28.9. HRMS (ESI): Calcd for $(M+H)^+$ ($C_{24}H_{22}ClN$) 394.1129, found 394.1123.

4.2 Virtual screening workflow

The crystal structure of the AR LBD domain (PDB entry: 2PNU) was assessed in our previous study and also used as the initial structure for the virtual screening in this study [24]. The grid box of the protein for SBVS was generated and centered on the co-crystallized ligand (EM-5744) in the LBP. The scaling factors for van der Waals interaction and the maximum partial atomic charges were set to 1.0 and 0.25,

respectively. Subsequently, the compounds (~200,000) in the Specs database were docked into the crystal structure of 2PNU, and the binding energies were scored and ranked by the Glide SP scoring mode [40]. After that, the top ranked 50,000 compounds were submitted to the Glide XP scoring, and the top ranked 10,000 compounds were rescored by the VD-MM/GBSA method [37]. The AM1-BCC charges were calculated for the ligands using the *sqm* module in *Amber 18* simulation package [41]. The protein-ligand systems were constructed using the antechamber and tleap modules in *Amber18* [41]. FF14SB force field and General Amber force field (GAFF) were assigned to the proteins and ligands, respectively [42, 43]. Each protein-ligand complex was immersed into a water box with a distance of 12 Å extended from any solute atom. Three phases of minimizations were performed to optimize each prepared system. At first, the whole protein and ligand were restrained by 5 kcal·mol^{-1}·Å^{-2} elastic constant for 10,000 cycles (5,000 steps of steepest descent and 5,000 steps of conjugate gradient minimizations). Thereafter, the backbone atoms of the protein were restrained by 5 kcal·mol^{-1}·Å^{-2} elastic constant for 10,000 cycles (5,000 steps of steepest descent and 5,000 steps of conjugate gradient minimizations). At last, the whole system was relaxed without any restraint for 10,000 cycles (5,000 steps of steepest descent and 5,000 steps of conjugate gradient minimizations). Subsequently, the optimized structures were submitted for the binding free energy calculations based on the VD-MM/GBSA method [37]. The top ranked 2,000 compounds were clustered based on the structural similarity using the *Canvas* module in Schrödinger [38]. Then, the binding poses of the clustered compounds were carefully checked and filtered. Finally, the compounds were carefully checked and filtered, and 32 compounds were purchased for subsequent bioassays.

4.3 MD simulation and VD-MM/GBSA of ***C18***

The system preparation of the AR LBD and **AT2** were processed by the protocol reported in our previous studies, including calculation of the partial charges for **AT2**, assignment of appropriate force field, addition of water molecules and ions, system

minimization, and MD heating and equilibrium [24, 44, 45]. Then the system was submitted to 1 μs MD simulation in the isothermal isobaric (NPT) ensemble. The *CPPTRAJ* module in *AmberTools* package for data analysis [46]. The last 0.2 μs MD simulation trajectory with 1000 snapshots was submitted to VD-MM/GBSA for free energy decomposition [37]. The VD-MM/GBSA calculations were performed by the *MMPBSA.py* module in *AmberTools* package by modifying the *sander* module to identify a new block of atomic dielectric constants in the revised AMBER system topology [37, 47]. The entropies were not considered because of the low prediction accuracy and expensive computational demand. The polar component of desolvation was estimated by the modified GB model (GB^{OBC1}) reported by Onufriev *et al* [48]. The exterior dielectric constant for solvent was set as default. The non-polar component of desolvation was computed using the LCPO algorithm [49].

4.4 AR transcriptional activity assay

LNCaP-ARR_2PB-eGFP was cultured in RPMI-1640 media, and the cells of LNCap were starved with 5% charcoal-stripped serum (CSS) for 5 days. Thereafter, the cells were plated into a 96-well plate with 3.5×10^4 cells/well, and continued to incubate at 37 □ in a 5% CO_2 atmosphere for 24 h. Then, 5 nM DHT and intended concentrations (10 μM for 32 compounds, 0-50 μM for **C18** and its analogues) of compounds were added to the prepared cells. Finally, the fluorescence intensities were determined after treatment for 3 days (Synergy H1, BioTek. Excitation, 485 nm; Emission, 535 nm).

4.5 Measurement of prostate-specific antigen (PSA)

After the AR transcriptional activity assay was finished, the media supernatant (300 μl) for each sample was sent to Cancer Hospital of University of Chinese Academy of Sciences, Zhejiang Cancer Hospital (Hangzhou, Zhejiang) to measure the secreted PSA using IMMULITE® 2000 XPi Immunoassay System (Siemens Ltd., Erlangen, Germany).

4.6 Competitive ligand binding assay

The PolarScreen™ Androgen Receptor Competitor Assay Kit (Invitrogen Life Technologies, Inc.) was utilized to determine the AR LBD binding affinity. Briefly, 10 μl 2× intended compounds (or DMSO, DHT, Enz) were dispersed in a low-volume 384-well plate. Then, 4× AR-LBD (GST) and 4× Fluormone AL (Flu-AL) Green dissolved in complete AR Green Assay Buffer were added. Afterwards, aluminized paper was used to protect the reagents from light, and after incubation for 4 h at room temperature, a multi-function plate reader (Synergy H1, BioTek, Winooski, VT) was used to measure the fluorescence polarization value (mP) for each well.

4.7 Cell proliferation assay

The cell proliferation for the cell lines of LNCAP, PC3, C4-2, and DU145 were evaluated by 3-(4,5-dimethyl-2-thiazolyl)-2,5-diphenyl-2-H-tetrazolium bromide (MTT) colorimetric assay. These cells were seeded in RPMI-1640 media (5% charcoal-stripped serum) with 1-5×10^3 cells/well in 96-well plates (3×10^3, 1.5×10^3, 1.5×10^3, and 1.5×10^3 cells/well for LNCaP, PC3, C4-2 and DU145, respectively). After incubation at 37 □ for 24 h, cells were then treated with 5nM DHT and serial dilutions of Enz and **AT2**, followed by incubation of 72 h. Then, each well was added with MTT (10 μl of 5 mg/ml) solutions and incubated for 4 h. After that, 100 μl of triplex 10% SDS-0.1% HCl-PBS solutions were added to dissolve the formazan crystals, and the plates were incubated overnight at 37 □. Finally, the absorbance at 570 nm was measured with the reference wavelength at 650 nm using a spectrophotometer (Eon, Bioteck, Winooski, VT).

4.8 Q-PCR

LNCaP cells were cultured in medium containing 5% charcoal-stripped serum (CSS) in six-well plates and treated with Enz, **AT2** (0.1, 1 or 10 μM), 5 nM DHT, or DMSO for 24 h. After 48 h of the treatment, mRNA were extracted using EZ-10 DNA away RNA Mini-Preps Kit (Sangon Biotech, Shanghai, China) and reversely transcribed

into cDNA using Hifair® □ 1st Strand cDNA Synthesis SuperMix for qPCR (YEASEN, Shanghai, China), and finally detected by qPCR with qPCR SYBR Green Master Mix (YEASEN, Shanghai, China). All the procedures followed the operation manuals (QuantStudio 3, Applied Biosystems, Graphpad Prism 7.0).

4.9 Immunofluorescence

LNCaP cells were cultured in 12-well plates containing coverslips and incubated at 37 □ for 24 h. 10 μM of **AT2** and Enz were individually added and then further incubated for 12 h, and then 5 nM DHT was added and incubated for 90 mins. Afterwards, the cells were fixed with 4 □ precooling 4% (vol/vol) paraformaldehyde, and permeabilized with Triton X-100. Then the cells were incubated with AR antibodies (#5153, Cell Signaling Technology) overnight after washing with PBS three times. An Alexa-488 conjugated goat-anti rabbit lgG (#4412, Cell Signaling Technology) diluted at 1:1000 was used as the secondary antibody. The counterstain 4',6-diamidino-2-phenylindole (DAPI) was utilized to visualize cell nucleus. The images were taken at 60 magnification using Nikon AR fluorescence microscope, followed by analysis with NIS-Elements Viewer (Northern Eclipse, Empix Imaging, Inc.).

4.10 *3T3 cytotoxicity assay*

3T3 cells were seeded with RPMI-1640 medium at a density of 3000/well. After the cells were attached, Enz, C18 and AT2 were seeded with various concentrations of less than 10 μM. After incubation at 37 □ for 24 h, the medium was sucked out, 100 μl DMSO was added into each well, and the absorbance was measured after shaking evenly for 5-10 minutes.

4.11 Statistical analysis

Data were analyzed statistically using the one-way analysis of variance test or Student's t-test via software of Graphpad prism 7.0 (GraphPad, San Diego, CA, USA).

Results were expressed as mean ± SEM with at least 3 replicates, and $P < 0.05$ was considered as significant.

Acknowledgments

This study was supported by National Key R&D Program of China (2016YFA0202900), Key R&D Program of Zhejiang Province (2020C03010), National Natural Science Foundation of China (21575128, 81773632), and Zhejiang Provincial Natural Science Foundation of China (LZ19H300001).

Reference

[1] F. Bray, J. Ferlay, I. Soerjomataram, R.L. Siegel, L.A. Torre, A. Jemal, Global cancer statistics 2018: GLOBOCAN estimates of incidence and mortality worldwide for 36 cancers in 185 countries, CA Cancer J Clin, 68 (2018) 394-424.

[2] D. Li, W. Zhou, J. Pang, Q. Tang, B. Zhong, C. Shen, L. Xiao, T. Hou, A magic drug target: androgen receptor, Med Res Rev, 39 (2019) 1485-1514.

[3] N. Elshan, M.B. Rettig, M.E. Jung, Molecules targeting the androgen receptor (AR) signaling axis beyond the AR-Ligand binding domain, Med Res Rev, 39 (2019) 910-960.

[4] A.A. Shafi, A.E. Yen, N.L.J.P. Weigel, therapeutics, Androgen receptors in hormone-dependent and castration-resistant prostate cancer, 140 (2013) 223-238.

[5] T.J. Maatman, M.K. Gupta, J.E. Montie, Effectiveness of castration versus intravenous estrogen therapy in producing rapid endocrine control of metastatic cancer of the prostate, J Urol, 133 (1985) 620-621.

[6] C. Cai, S.P. Balk, Intratumoral androgen biosynthesis in prostate cancer pathogenesis and response to therapy, Endocr Relat Cancer, 18 (2011) R175-182.

[7] M.H. Tan, J. Li, H.E. Xu, K. Melcher, E.L. Yong, Androgen receptor: structure, role in prostate cancer and drug discovery, Acta Pharmacol Sin, 36 (2015) 3-23.

[8] D. Leveque, Enzalutamide in metastatic prostate cancer, N Engl J Med, 381 (2019) 1494.

[9] P.A. Watson, V.K. Arora, C.L. Sawyers, Emerging mechanisms of resistance to androgen receptor inhibitors in prostate cancer, Nat Rev Cancer, 15 (2015) 701-711.

[10] J.M. van Dodewaard-de Jong, H.M.W. Verheul, H.J. Bloemendal, J.M.H. de Klerk, M.A. Carducci, A.J.M. van den Eertwegh, New treatment options for patients with metastatic prostate cancer: what is the optimal sequence?, Clin Genitourin Cancer, 13 (2015) 271-279.

[11] M.R. Smith, E.S. Antonarakis, C.J. Ryan, W.R. Berry, N.D. Shore, G. Liu, J.J. Alumkal, C.S. Higano, E. Chow Maneval, R. Bandekar, C.J. de Boer, M.K. Yu, D.E. Rathkopf, Phase 2 study of the safety and antitumor activity of apalutamide (ARN-509), a potent androgen receptor antagonist, in the high-risk nonmetastatic castration-resistant prostate cancer cohort, Eur Urol, 70 (2016) 963-970.

[12] J.D. Joseph, N. Lu, J. Qian, J. Sensintaffar, G. Shao, D. Brigham, M. Moon, E.C. Maneval, I. Chen,

B. Darimont, J.H. Hager, A clinically relevant androgen receptor mutation confers resistance to second-generation antiandrogens enzalutamide and ARN-509, Cancer Discov, 3 (2013) 1020-1029.

[13] T. Hara, J. Miyazaki, H. Araki, M. Yamaoka, N. Kanzaki, M. Kusaka, M. Miyamoto, Novel mutations of androgen receptor: a possible mechanism of bicalutamide withdrawal syndrome, Cancer Res, 63 (2003) 149-153.

[14] M.S. Ozers, B.D. Marks, K. Gowda, K.R. Kupcho, K.M. Ervin, T. De Rosier, N. Qadir, H.C. Eliason, S.M. Riddle, M.S. Shekhani, The androgen receptor T877A mutant recruits LXXLL and FXXLF peptides differently than wild-type androgen receptor in a time-resolved fluorescence resonance energy transfer assay, Biochemistry, 46 (2007) 683-695.

[15] K. Steketee, L. Timmerman, A.C. Ziel-van der Made, P. Doesburg, A.O. Brinkmann, J. Trapman, Broadened ligand responsiveness of androgen receptor mutants obtained by random amino acid substitution of H874 and mutation hot spot T877 in prostate cancer, Int J Cancer, 100 (2002) 309-317.

[16] M. Bassetto, S. Ferla, F. Pertusati, S. Kandil, A.D. Westwell, A. Brancale, C. McGuigan, Design and synthesis of novel bicalutamide and enzalutamide derivatives as antiproliferative agents for the treatment of prostate cancer, Eur J Med Chem, 118 (2016) 230-243.

[17] A.V. Ivachtchenko, Y.A. Ivanenkov, O.D. Mitkin, A.A. Vorobiev, I.V. Kuznetsova, N.A. Shevkun, A.G. Koryakova, R.N. Karapetian, A.S. Trifelenkov, D.V. Kravchenko, M.S. Veselov, N.V. Chufarova, Design, synthesis and biological evaluation of novel 5-oxo-2-thioxoimidazolidine derivatives as potent androgen receptor antagonists, Eur J Med Chem, 99 (2015) 51-66.

[18] M. Zuo, X. Xu, Z. Xie, R. Ge, Z. Zhang, Z. Li, J. Bian, Design and synthesis of indoline thiohydantoin derivatives based on enzalutamide as antiproliferative agents against prostate cancer, Eur J Med Chem, 125 (2017) 1002-1022.

[19] J. Zhou, G. Geng, Q. Shi, F. Sauriol, J.H. Wu, Design and synthesis of androgen receptor antagonists with bulky side chains for overcoming antiandrogen resistance, J Med Chem, 52 (2009) 5546-5550.

[20] C.A. Lipinski, Lead- and drug-like compounds: the rule-of-five revolution, Drug Discov Today Technol, 1 (2004) 337-341.

[21] C.H. Song, S.H. Yang, E. Park, S.H. Cho, E.Y. Gong, D.B. Khadka, W.J. Cho, K. Lee, Structure-based virtual screening and identification of a novel androgen receptor antagonist, J Biol Chem, 287 (2012) 30769-30780.

[22] H. Li, X. Ren, E. Leblanc, K. Frewin, P.S. Rennie, A. Cherkasov, Identification of novel androgen receptor antagonists using structure- and ligand-based methods, J Chem Inf Model, 53 (2013) 123-130.

[23] L. Wang, T. Song, X. Wang, J. Li, Discovery and identification of pyrazolopyramidine analogs as novel potent androgen receptor antagonists, Front Pharmacol, 9 (2018) 864.

[24] W. Zhou, M. Duan, W. Fu, J. Pang, Q. Tang, H. Sun, L. Xu, S. Chang, D. Li, T. Hou, Discovery of novel androgen receptor ligands by structure-based virtual screening and bioassays, Genomics Proteomics Bioinformatics, 16 (2018) 416-427.

[25] S. Forli, R. Huey, M.E. Pique, M.F. Sanner, D.S. Goodsell, A.J. Olson, Computational protein-ligand docking and virtual drug screening with the AutoDock suite, Nat Protoc, 11 (2016) 905-919.

[26] M. Zheng, J. Zhao, C. Cui, Z. Fu, X. Li, X. Liu, X. Ding, X. Tan, F. Li, X. Luo, K. Chen, H. Jiang,

Computational chemical biology and drug design: Facilitating protein structure, function, and modulation studies, Med Res Rev, 38 (2018) 914-950.

[27] Z. Wang, H. Sun, X. Yao, D. Li, L. Xu, Y. Li, S. Tian, T. Hou, Comprehensive evaluation of ten docking programs on a diverse set of protein-ligand complexes: the prediction accuracy of sampling power and scoring power, Phys Chem Chem Phys, 18 (2016) 12964-12975.

[28] C.N. Cavasotto, N.S. Adler, M.G. Aucar, Quantum chemical approaches in structure-based virtual screening and lead optimization, Front Chem, 6 (2018) 188.

[29] I.A. Guedes, F.S.S. Pereira, L.E. Dardenne, Empirical scoring functions for structure-based virtual screening: applications, critical aspects, and challenges, Front Pharmacol, 9 (2018) 1089.

[30] J. Li, A. Fu, L. Zhang, An overview of scoring functions used for protein-ligand interactions in molecular docking, Interdiscip Sci, 11 (2019) 320-328.

[31] S. Genheden, U. Ryde, The MM/PBSA and MM/GBSA methods to estimate ligand-binding affinities, Expert Opin Drug Discov, 10 (2015) 449-461.

[32] S.I. Virtanen, S.P. Niinivehmas, O.T. Pentikainen, Case-specific performance of MM-PBSA, MM-GBSA, and SIE in virtual screening, J Mol Graph Model, 62 (2015) 303-318.

[33] E. Wang, H. Sun, J. Wang, Z. Wang, H. Liu, J.Z.H. Zhang, T. Hou, End-point binding free energy calculation with mm/pbsa and mm/gbsa: Strategies and applications in drug design, Chem Rev, 119 (2019) 9478-9508.

[34] X. Liu, L. Peng, J.Z. Zhang, Accurate and efficient calculation of protein-protein binding free energy-interaction entropy with residue type specific dielectric constants, J. Chem. Inf. Model., (2018) doi: 10.1021/acs.jcim.1028b00248.

[35] T. Venken, D. Krnavek, J. Munch, F. Kirchhoff, P. Henklein, M. De Maeyer, A. Voet, An optimized MM/PBSA virtual screening approach applied to an HIV-1 gp41 fusion peptide inhibitor, Proteins, 79 (2011) 3221-3235.

[36] I.S. Moreira, P.A. Fernandes, M.J. Ramos, Computational alanine scanning mutagenesis--an improved methodological approach, J Comput Chem, 28 (2007) 644-654.

[37] E. Wang, G. Weng, H. Sun, H. Du, F. Zhu, F. Chen, Z. Wang, T. Hou, Assessing the performance of the MM/PBSA and MM/GBSA methods. 10. Impacts of enhanced sampling and variable dielectric model on protein-protein Interactions, Phys Chem Chem Phys, 21 (2019) 18958-18969.

[38] S.J.L.N.Y. Canvas, NY, USA, version 3.1. 011, (2017).

[39] H. Borgmann, N. Lallous, D. Ozistanbullu, E. Beraldi, N. Paul, K. Dalal, L. Fazli, A. Haferkamp, P. Lejeune, A. Cherkasov, M.E. Gleave, Moving towards precision urologic oncology: targeting enzalutamide-resistant prostate cancer and mutated forms of the androgen receptor using the novel inhibitor darolutamide (ODM-201), Eur Urol, 73 (2018) 4-8.

[40] L.J.S. Schrödinger, LLC: New York, NY, USA, Glide, (2017).

[41] T.-S. Lee, D.S. Cerutti, D. Mermelstein, C. Lin, S. LeGrand, T.J. Giese, A. Roitberg, D.A. Case, R.C. Walker, D.M.J.J.o.c.i. York, modeling, GPU-accelerated molecular dynamics and free energy methods in Amber18: performance enhancements and new features, 58 (2018) 2043-2050.

[42] J. Wang, R.M. Wolf, J.W. Caldwell, P.A. Kollman, D.A. Case, Development and testing of a general amber force field, Journal of computational chemistry, 25 (2004) 1157-1174.

[43] J.A. Maier, C. Martinez, K. Kasavajhala, L. Wickstrom, K.E. Hauser, C. Simmerling, ff14SB: improving the accuracy of protein side chain and backbone parameters from ff99SB, J Chem

Theory Comput, 11 (2015) 3696-3713.

[44] M. Duan, N. Liu, W. Zhou, D. Li, M. Yang, T. Hou, Structural diversity of ligand-binding androgen receptors revealed by microsecond long molecular dynamics simulations and enhanced sampling, J Chem Theory Comput, 12 (2016) 4611-4619.

[45] N. Liu, W. Zhou, Y. Guo, J. Wang, W. Fu, H. Sun, D. Li, M. Duan, T. Hou, Molecular dynamics simulations revealed the regulation of ligands to the interactions between androgen receptor and its coactivator, J Chem Inf Model, 58 (2018) 1652-1661.

[46] D.R. Roe, T.E. Cheatham, 3rd, PTRAJ and CPPTRAJ: software for processing and analysis of molecular dynamics trajectory data, J Chem Theory Comput, 9 (2013) 3084-3095.

[47] B.R. Miller, 3rd, T.D. McGee, Jr., J.M. Swails, N. Homeyer, H. Gohlke, A.E. Roitberg, MMPBSA.py: an efficient program for end-state free energy calculations, J. Chem. Theory Comput., 8 (2012) 3314-3321.

[48] A. Onufriev, D. Bashford, D.A. Case, Modification of the generalized Born model suitable for macromolecules, J Phys Chem B, 104 (2000) 3712-3720.

[49] J. Weiser, P.S. Shenkin, W.C. Still, Approximate atomic surfaces from linear combinations of pairwise overlaps (LCPO), Journal of Computational Chemistry, 20 (1999) 217-230.

Journal Pre-proof

Figure Legends

Figure 1. The schematic workflow of SBVS.

Figure 2. Biological evaluation of the compounds identified by VS. (A) LNCaP-ARR$_2$PB-eGFP-based transcriptional activity assay to determine the antagonistic activities for the 32 tested compounds (10 μM); (B) PolarScreen^{TM} AR competitor assay to assess the AR binding affinities of the 3 identified active compounds (10 μM); (C) The AR binding affinity of the hit **C18**; (D) Transcriptional activity assay of **C18**; (E) **C18** reduces the PSA expression in LNCap cells.

Figure 3. Rational design of the **C18** analogues. (A) RMSDs of the backbone atoms

of the AR LBD and the heavy atoms of **C18** as a function of MD simulation time; (B) The 10 key residues for the binding of **C18** predicted by VD-MM/GBSA. (C) Structural analysis of the 10 key residues for the interactions between the AR LBD and **C18**.

Figure 4. **AT2** can target the AR-LBD and reduce the PSA expression. (A) PolarScreen^{TM} AR Competitor Assay to assess the **C18** analogues (10 μM); (B) **AT2** reduces the PSA expression in LNCap cells with a dose-dependent fashion; (C) The relative mRNA expression of PSA; (D) The relative mRNA expression of TMPSS2; (E) Cytotoxicity assay effects of Enz, **C18** and **AT2** against NIH-3T3 cells.

Figure 5. **AT2** inhibits the AR nuclear translocation induced by DHT (scale bar = 50 μm).

Figure 6. Antiproliferative effects of Enz, **C18**, and **AT2** against the cells of (A) LNCap, (B) PC3, (C) C4-2, and (D) DU145 were determined by MTT assay. The cells were treated by different concentrations of the tested compounds for 72 h.

Journal Pre-proof

Table 1. IC_{50} (μM) of the 21 analogues of C18 determined by transcriptional activity assay.

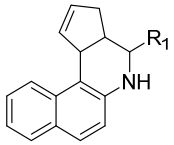

AT1-AT8

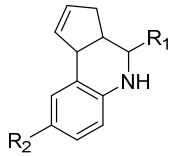

BT1-BT7

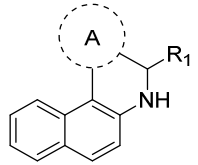

CT1-CT6

Comp.	R_1	IC_{50} (μM)	Comp.	R_1	R_2	IC_{50} (μM)	Comp.	R_1	A	IC_{50} (μM)
AT1		0.22	**BT1**		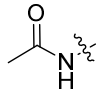	N/A	**CT1**		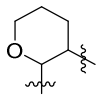	N/A
AT2	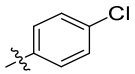	0.15	**BT2**	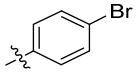	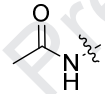	N/A	**CT2**	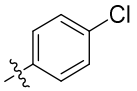	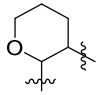	N/A
AT3	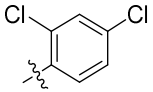	N/A	**BT3**	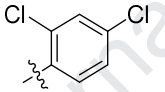	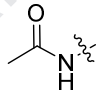	N/A	**CT3**	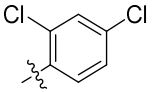	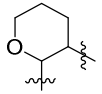	20.35
AT4	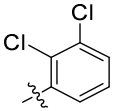	0.82	**BT4**	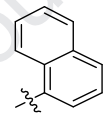	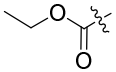	N/A	**CT4**		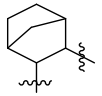	5.60
AT5	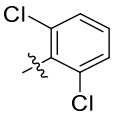	1.92	**BT5**	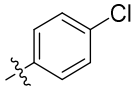	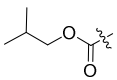	N/A	**CT5**	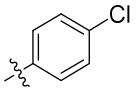	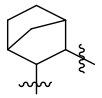	7.45
AT6	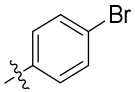	0.15	**BT6**	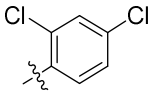	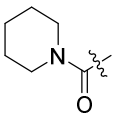	N/A	**CT6**	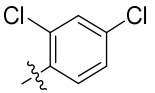	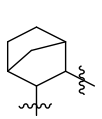	N/A

Journal Pre-proof

AT7	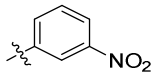	0.26	**BT7**	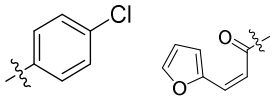	N/A		
AT8	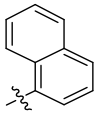	0.69	**C18**		2.40	**Enz**	0.036

Note: N/A means not applicable

Journal Pre-proof

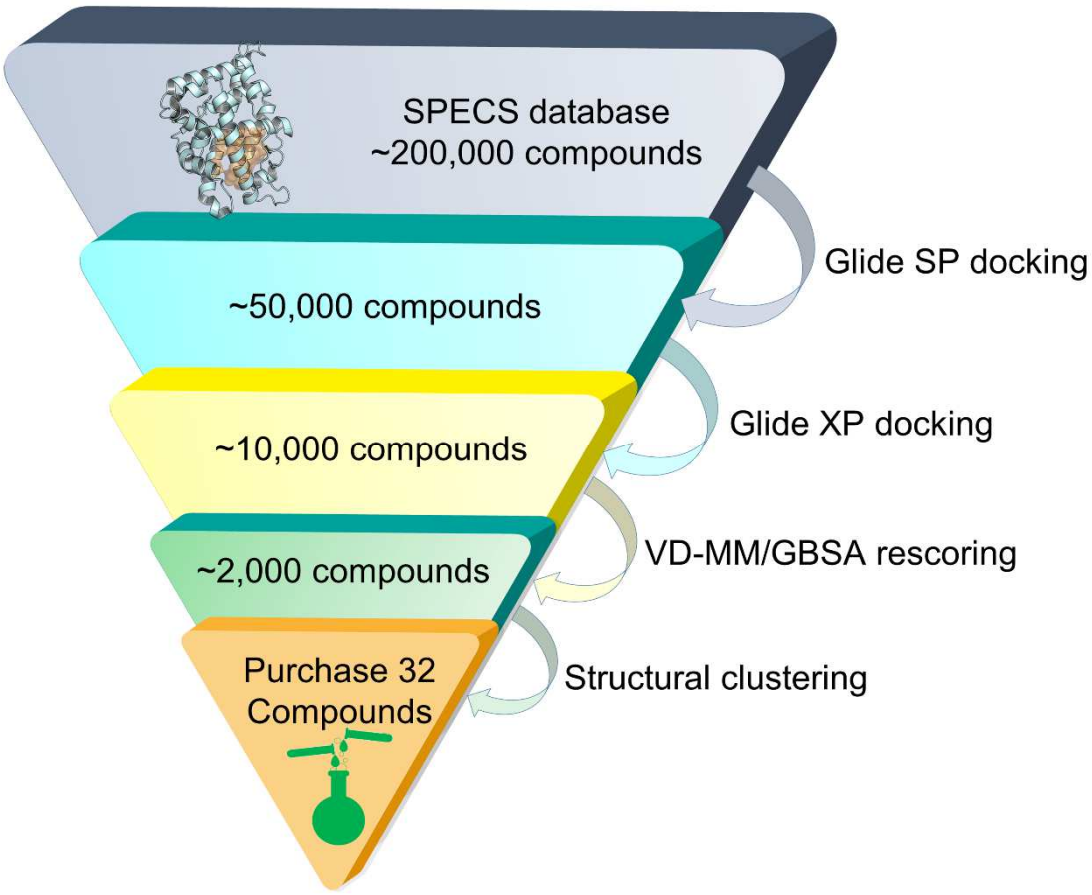

Figure 1

Journal

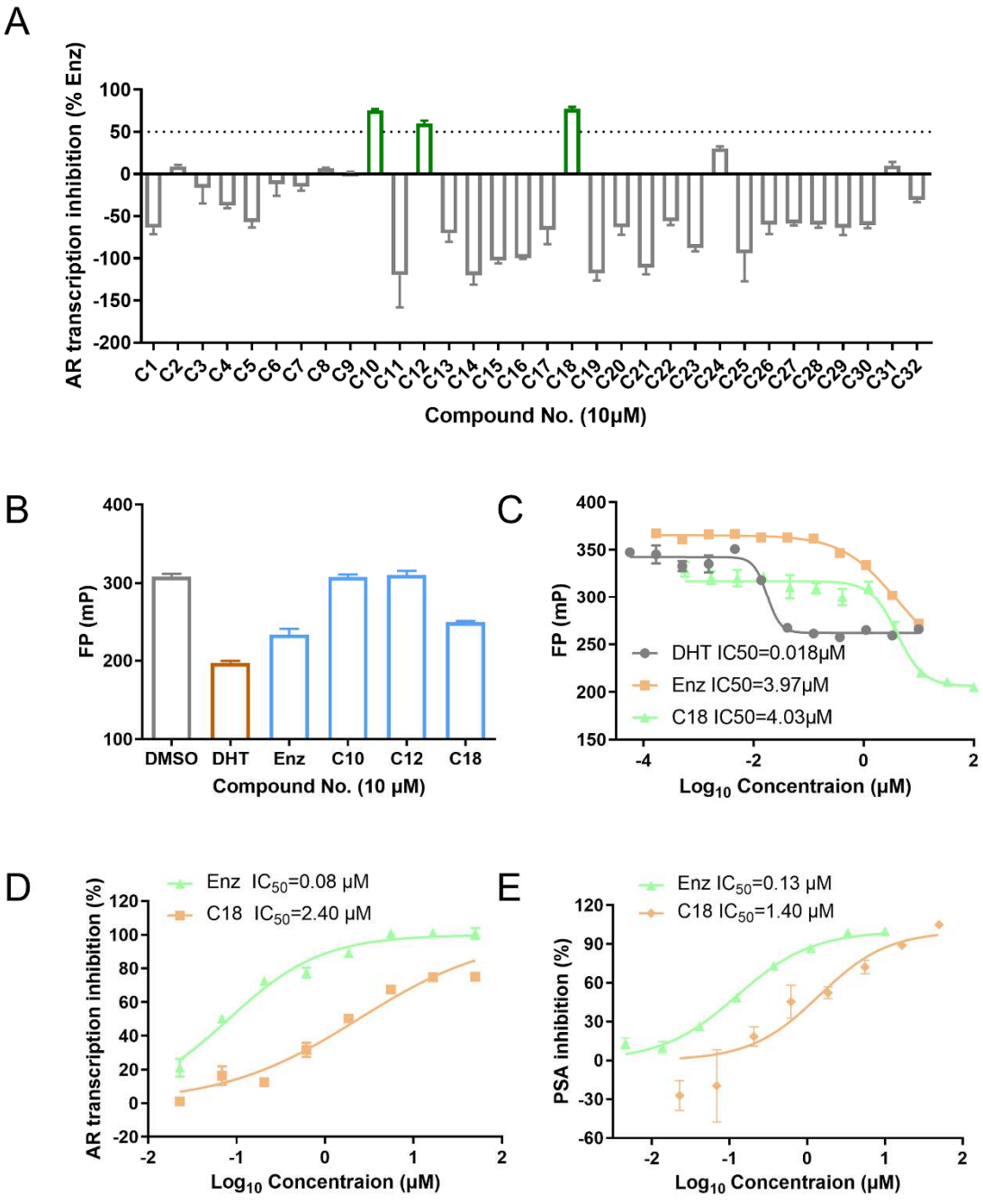
A
AR transcription inhibition (% Enz)
100
50
0
-50
-100
-150
-200
C1 C2 C3 C4 C5 C6 C7 C8 C9 C10 C11 C12 C13 C14 C15 C16 C17 C18 C19 C20 C21 C22 C23 C24 C25 C26 C27 C28 C29 C30 C31 C32
Compound No. (10μM)
B
FP (mP)
400
300
200
100
DMSO DHT Enz C10 C12 C18
Compound No. (10 μM)
C
FP (mP)
400
350
300
250
200
150
DHT IC50=0.018μM
Enz IC50=3.97μM
C18 IC50=4.03μM
-4 -2 0 2
Log10 Concentraion (μM)
D
AR transcription inhibition (%)
Enz IC50=0.08 μM
C18 IC50=2.40 μM
120
100
80
60
40
20
0
-20
-2 -1 0 1 2
Log10 Concentraion (μM)
E
PSA inhibition (%)
Enz IC50=0.13 μM
C18 IC50=1.40 μM
120
90
60
30
0
-30
-60
-2 -1 0 1 2
Log10 Concentraion (μM)

Figure 2

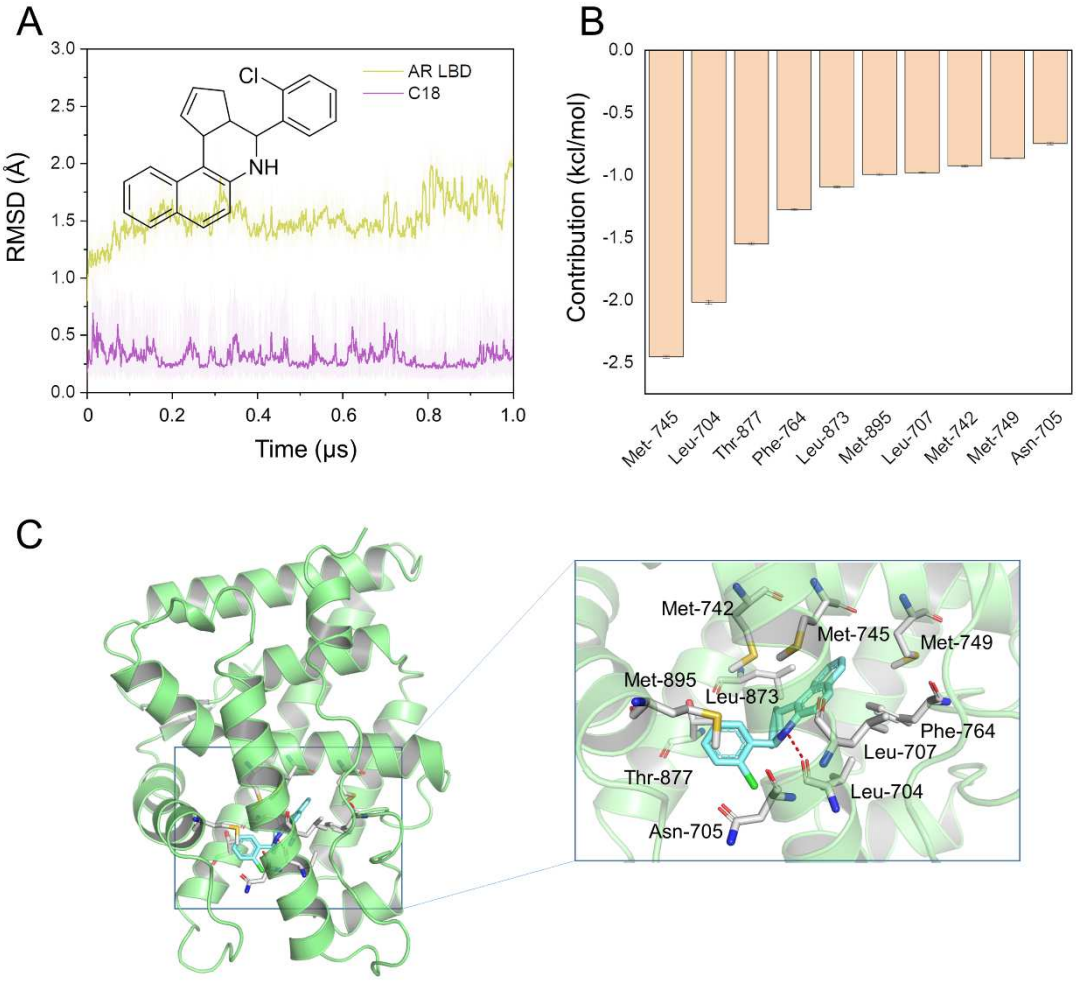
A
RMSD (Å)
Time (μs)
AR LBD
C18
Cl
NH
B
Contribution (kcl/mol)
Met- 745
Leu-704
Thr-877
Phe-764
Leu-873
Met-895
Leu-707
Met-742
Met-749
Asn-705
C
Met-742
Met-745
Met-749
Met-895
Leu-873
Phe-764
Leu-707
Thr-877
Leu-704
Asn-705

Figure 3

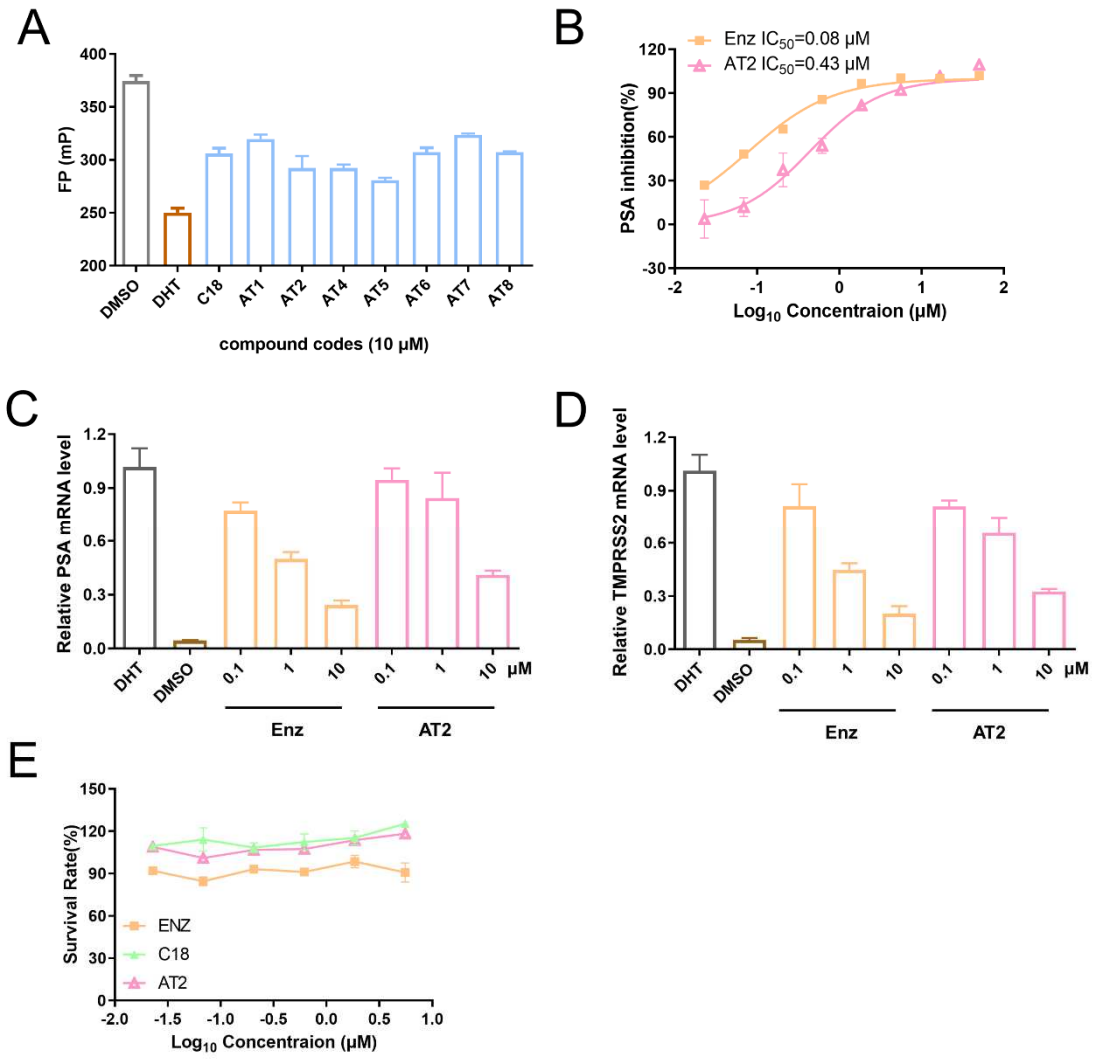
A
FP (mP)
400
350
300
250
200
DMSO
DHT
C18
AT1
AT2
AT4
AT5
AT6
AT7
AT8
compound codes (10 μM)
B
Enz IC50=0.08 μM
AT2 IC50=0.43 μM
PSA inhibition(%)
120
90
60
30
0
-30
-2
-1
0
1
2
Log10 Concentraion (μM)
C
Relative PSA mRNA level
1.2
0.9
0.6
0.3
0.0
DHT
DMSO
0.1
1
10
0.1
1
10
μM
Enz
AT2
D
Relative TMPRSS2 mRNA level
1.2
0.9
0.6
0.3
0.0
DHT
DMSO
0.1
1
10
0.1
1
10
μM
Enz
AT2
E
Survival Rate(%)
150
120
90
60
30
0
ENZ
C18
AT2
-2.0
-1.5
-1.0
-0.5
0.0
0.5
1.0
Log10 Concentraion (μM)

Figure 4

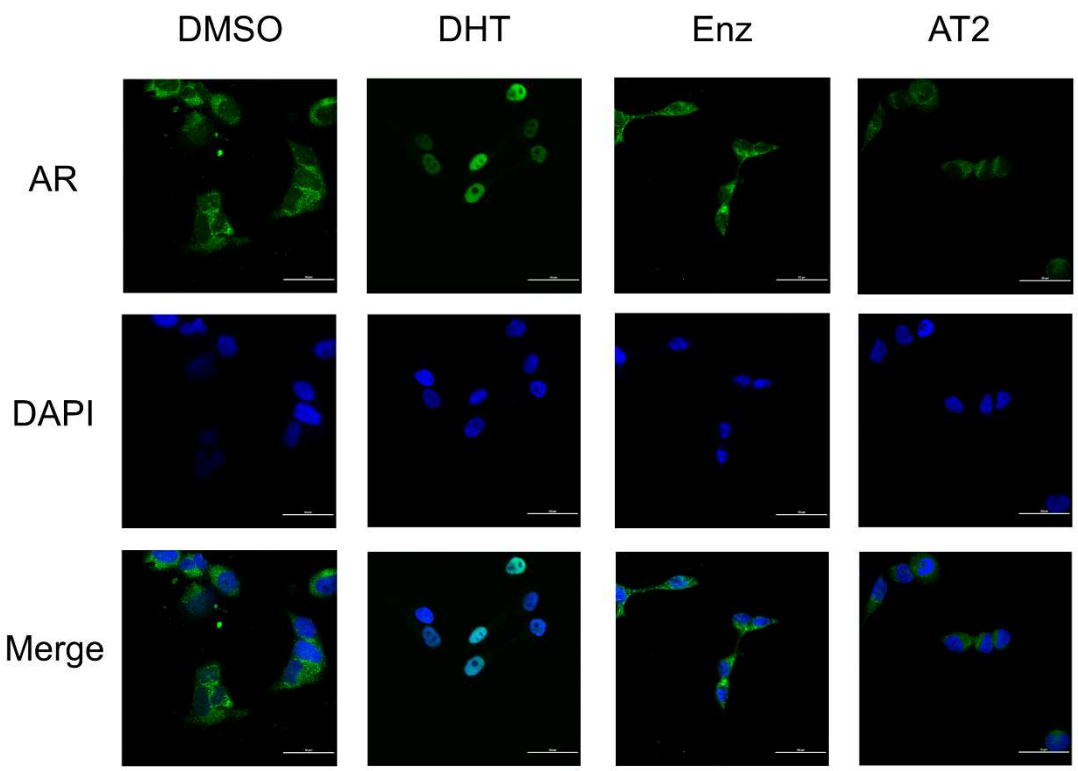

Figure 5

Journal Pre-proof

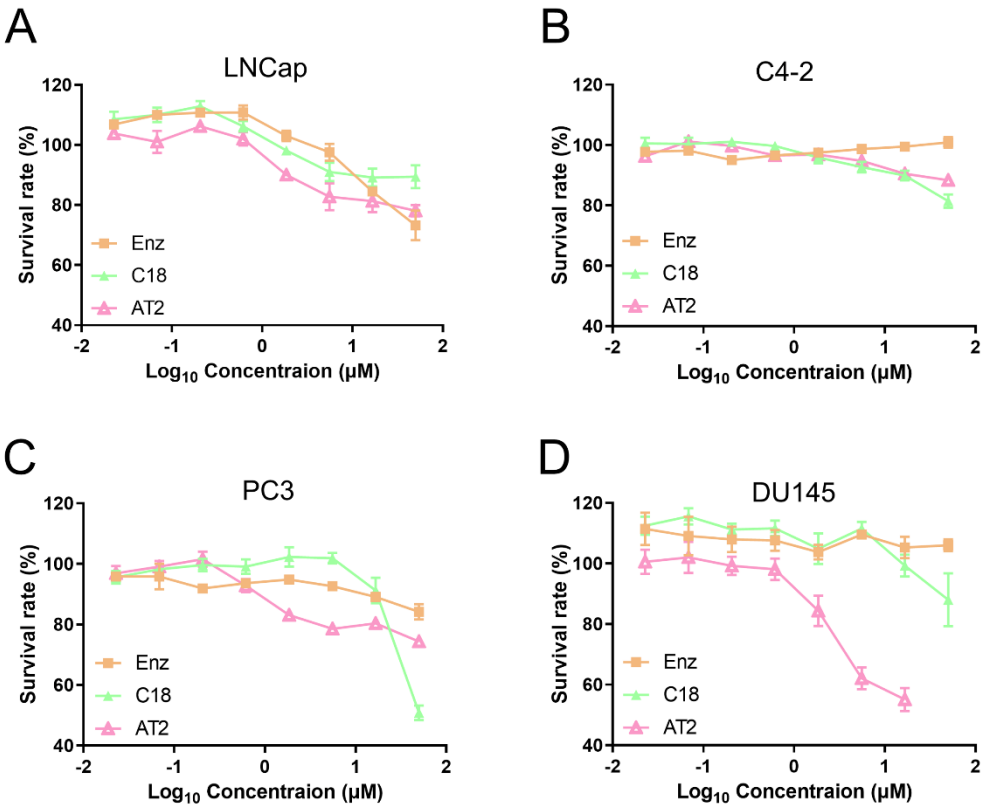

Figure 6

Journal Pre-proof

Journal Pre-proof

Highlights

1. A novel hit (**C18**) with IC_{50} of 2.4 μM against AR transcriptional activity in LNCaP cell was identified through structure-based virtual screening.
2. The SAR analysis and structural optimization of **C18** resulted in the discovery of a more potent AR antagonist (**AT2**) with 16-fold improved anti-AR potency.
3. Further assays indicated that **AT2** could effectively inhibit the transcriptional function of AR and block the nuclear translocation of AR.

Journal Pre-proof

Journal Pre-proof

Declaration of interests

☒ The authors declare that they have no known competing financial interests or personal relationships that could have appeared to influence the work reported in this paper.

☐The authors declare the following financial interests/personal relationships which may be considered as potential competing interests:

Journal Pre-proof